Characterization of Supramolecular Polyphenol−Chromium(III) Clusters by Molecular Dynamics Simulations

Simona Bronco,[†] Chiara Cappelli,*[,†] and Susanna Monti*[,‡]

Istituto per i Processi Chimico-Fisici (IPCF-CNR), Area della Ricerca, via G. Moruzzi 1, I-56124 Pisa, Italy, and PolyLab-CNR, and Dipartimento di Chimica e Chimica Industriale, Università degli Studi di Pisa, Via Risorgimento 35, I-56126 Pisa, Italy

Received: March 22, 2006; In Final Form: May 11, 2006

The binding of Cr(III) with (2R,3S,4R)-(+)-3,3′,4,4′,7-flavanpentol in aqueous solution is investigated by atomistic molecular dynamics simulations concentrating the analysis of the sampled data on the polyphenol ability to chelate metal ions and to form large noncovalently bonded molecular and supramolecular architectures.

1. Introduction

In a previous study of ours, the conformational and chiroptical properties of (2R,3S,4R)-(+)-3,3′,4,4′,7-flavanpentol (FLA) (Figure 1), its binding to collageniclike peptides, and the influence of the surrounding environment on the conformational properties and ultraviolet/circular dichroism (UV/CD) spectra of this molecule were investigate by ab initio calculations and molecular dynamics (MD) simulations in solution.[1] In this paper, the ability of FLA to interact with chromium(III) ions in water solution is explored through classical MD simulations starting from the minimum energy conformations already identified.

The group of polyphenol compounds, which FLA is a member of, are known to form coordination complexes with metal ions including chromium.[2] Chromium salts are used worldwide in tanning processes, and current leather industry technology is dominated by chromium(III).[3] However, chrome tanning alone is insufficient to provide the aesthetic requirements, such as color, strength, and softness, for the wide range of leather types produced. Therefore, the industry has resorted to other tannages, namely, polyphenols (vegetable tannins), which were the main compounds employed in traditional tanning methodologies, to complement chromium.

Unfortunately, during the tanning process, both chromium and polyphenol uptake is not complete and gives rise to the waste of materials. Vegetable tannins are considered ecofriendly molecules because of their natural origin; chromium(III), by contrast, may be toxic due to its possible conversion to chromium(VI) under appropriate environmental conditions. Chromium(VI) is a human carginogen that predominates in contaminated soils and waters as mobile anions. Due to their chelating properties, vegetable tannins could be successfully used in the design of highly efficient and selective materials for the removal and separation of toxic and environmentally relevant Cr(III) ions. The presence of several hydroxyl groups in their structures makes them reactive to forming selective and directional hydrogen bonds indispensable for the construction and stabilization of large noncovalently bonded molecular and supramolecular architectures. The synergistic effect of hydrogen bonding and hydrophobic association, manifested also in their interaction with collagen microfibril segments, has been evidenced by experimental data and computational studies of ours[1,4,5] which succeeded in elucidating and rationalizing the observed increase in hydrothermal stability of collagen molecules and in identifying the preferred binding sites and dominant mode of their interaction. The aim of this paper is to suggest possible flavonoid−metal ions interaction mechanisms in solution through the intricate characterization of the molecular cluster sampled during nanosecond MD production runs. Recent computational studies mainly focus on Cr(III) ion's hydration structure,[6−8] the modeling of possible polynuclear chromium complexes in solution,[9] and the stereochemical analysis of complexes made of Cr(III) and EDTA-type molecules.[10,11] However, to the best of our knowledge, no molecular dynamics exploration of polyphenol−Cr(III) aggregation in solution has yet been reported.

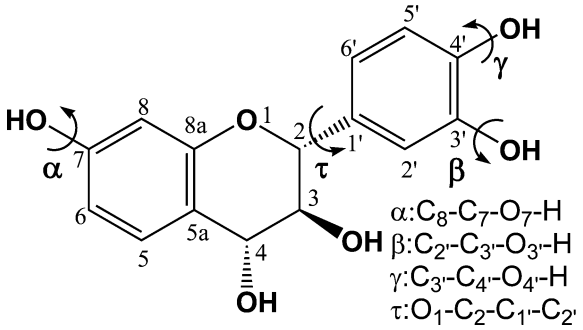

Figure 1. (2R,3S,4R)-(+)-3,3′,4,4′,7-flavanpentol (FLA) structure and definition of the dihedral angles analyzed during the MD simulation runs.

2. Computational Details

2.1. Ab Initio Calculation and Force Field Parameters. Initial setup and MD runs were performed with the AMBER8[12] package running on the IBM Linux cluster 1350 (CLX) at CINECA. The electrostatic and van der Waals interactions were described within a pairwise additive scheme by the usual coulomb term with a dielectric permittivity constant equal to 1 and the 6-12 Lennard−Jones potential. Parameters for FLA molecules and Cl^- counterions were taken from the general amber force field (GAFF) and previous studies of ours,[1,4,5]

* Authors to whom correspondence should be addressed. Phone: +39-050-2219293 (C.C.); +39-050-3152520 (S.M.). Fax: +39-050-2219260 (C.C.); +39-050-3152442 (S.M.). E-mail: chiara@dcci.unipi.it (C.C.); s.monti@ipcf.cnr.it (S.M.).

† PolyLab-CNR.

‡ Istituto per i Processi Chimico-Fisici (IPCF-CNR).

10.1021/jp061776a CCC: $33.50 © 2006 American Chemical Society
Published on Web 06/09/2006

whereas Cr^{3+} parameters were derived from ref 13 and subsequently modified to reproduce the molecular geometries of three representative model aggregates, that is, (**1**) $[Cr(H_2O)_6]^{3+}$, (**2**) $[Cr(H_2O)_5CH_3OH]^{3+}$, and (**3**) $[Cr(H_2O)_5C_2H_4]^{3+}$. The initial geometries of the chosen Cr^{3+} complexes were built starting from the six-coordinated octahedron structure assumed for **1**, which is in accordance with the X-ray diffraction data,[14] substituting one water molecule with a CH_3OH molecule in model **2** and with a C_2H_4 molecule in model **3**. The OH group of CH_3OH was superimposed to one OH group of the removed water molecule, whereas the C_2H_4 molecule was placed with both its carbon atoms at a distance of ≈2.2 Å from the Cr^{3+} ion. Optimization of the selected complexes using the density functional theory method were carried out with the Gaussian03 quantum chemistry suite of programs.[15] The B3LYP functional, the triple-ζ 6-311++G(p,d) basis set for the Cr^{3+} ion, and the aug-cc-pVDZ basis set for the rest of the atoms were used in all the calculations. Force field empirical parameters for Cr^{3+} were adjusted to get the best possible match between the molecular mechanics (MM) calculated and ab initio optimized structural data of the three Cr^{3+} complexes. A fairly good reproduction of the ab initio structures (root-mean-square deviation lower than 0.2 Å) was achieved using Cr^{3+} Lennard−Jones parameters ϵ and r^* equal to 0.25 kcal/mol and 1.12 Å, respectively. Superimposed geometries of the three models are displayed in Figure 2.

2.2. Molecular Dynamics Simulation Protocols. Two systems were generated for simulation. The first one, hereafter called the reduced system (RedSy), consisted of one FLA molecule with 6 Cr^{3+} ions placed near each FLA oxygen atom at a distance of about 2 Å and 18 charge balancing Cl^- counterions surrounded by 530 water molecules. The second one, hereafter called the extended system (ExtSy), consisted of 57 FLA molecules with 50 Cr^{3+} ions and 150 charge balancing Cl^- counterions surrounded by 3414 water molecules. For both models, the Cl^- counterions were added to neutralize Cr^{3+} charges, randomly placed, in the second case, near FLA molecules, using the standard AMBER8 programs which explore the electrostatic energy surface in the space around the Cr^{3+} ions to find counterion positions with favorable counterion−ion interactions. Water was described by the TIP3P model,[16] and energy minimization, molecular dynamics equilibration, and production runs were performed using the all-atom GAFF. Long-range electrostatic interactions were treated with the particle mesh Ewald (PME) method and nonbonded interactions were truncated at 9 Å for RedSy and at 12 Å for ExtSy. Periodic boundary conditions were applied in all simulations via both nearest image and the discrete Fourier transform, implemented as part of the PME method. All bonds involving hydrogen atoms were restrained using the SHAKE algorithm,[17] and the time step was set to 1 fs. The starting structures were first energy minimized to remove bad steric interactions, and then, while keeping the FLA atoms, Cr^{3+} ions, and Cl^- counterions fixed, the models were heated gradually to 600 K during 50 ps and then cooled gradually to 305 K during 30 ps while holding both the volume and temperature constant (NVT ensemble) in order to randomize water positions. The resulting conformations were subjected to a further equilibration protocol coupling each system to a thermal bath of temperature $T = 305$ K and to a pressure bath of pressure $P = 1$ atm for a total period of 100 ps to allow density adjustment. During this time interval, solute heavy atoms were restrained by a harmonic potential with a starting force constant of 100 kcal/(mol Å^2) which was slowly reduced to zero. In fact, in the subsequent production stage,

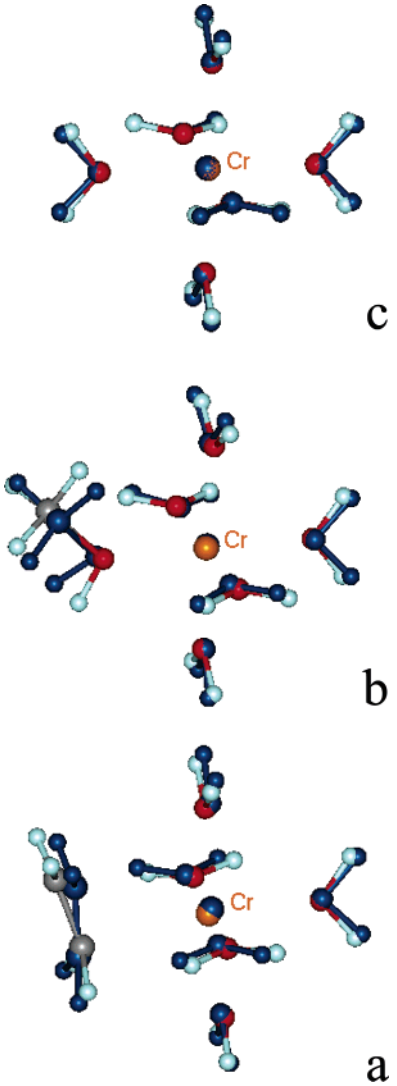

Figure 2. Superimposed ab initio optimized geometries of (a) $[Cr(H_2O)_5C_2H_4]^{3+}$, (b) $[Cr(H_2O)_5CH_3OH]^{3+}$, and (c) $[Cr(H_2O)_6]^{3+}$ with the corresponding MM optimized ones. The MM structures are shown in blue.

performed in the NPT ensemble using a Berendsen coupling scheme,[18] all atoms in the system were allowed to move. The first 1 ns of trajectories of the production run were excluded from the final analysis and considered as part of the equilibration phase. A production run of 10 ns for RedSy and a simulation of 6.7 ns for ExtSy were carried out. Configurations were stored every 1 ps giving a total of 10 000 and 6700 saved structures for RedSy and ExtSy, respectively.

3. Results and Discussion

Atomic positions collected every picosecond were used to build radial pair distribution functions chosen to characterize solvated Cr^{3+} ions ($g_{Cr-OW}(r)$ and $g_{Cr-Cl}(r)$), to determine their most probable FLA interaction sites ($g_{Cr-O_i}(r)$, $i = 1, 3, 4, 7, 3', \text{and } 4'$), and to depict the water arrangement around FLA molecules ($g_{OW-O_i}(r)$, $i = 1, 3, 4, 7, 3', \text{and } 4'$). As a more general description, two center-of-mass pair distribution functions, FLA−Cr^{3+} and FLA−water (WAT), are also reported together with residence times for the different solute−solvent interacting sites. FLA structural behavior in solution is delineated through its four torsion angle distributions and compared with the results obtained by the study of its interactions, in water

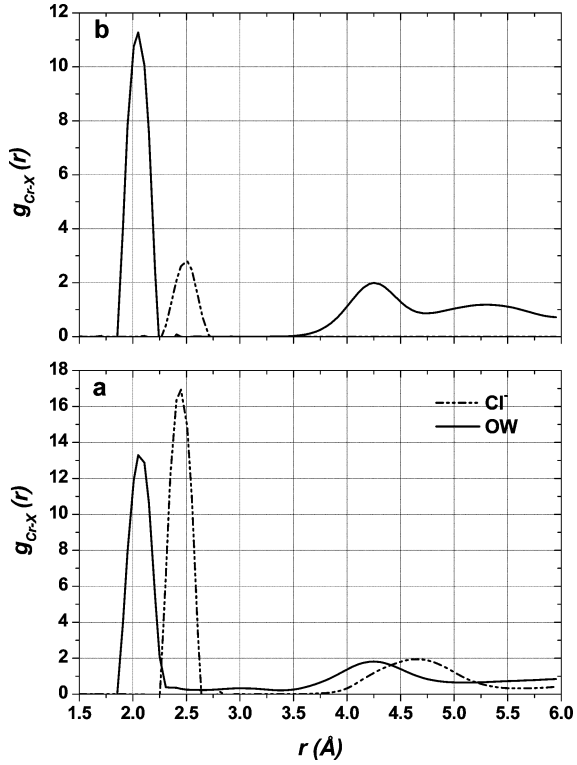

Figure 3. Cr^{3+}−water oxygen (OW) and Cr^{3+}−Cl^- radial distribution functions for (a) RedSy and (b) ExtSy.

solution, with a collagenlike peptide microfibril segment. FLA self-association is characterized through the analysis of the hydrogen bonding network.

3.1. Radial Distribution Functions. It has been demonstrated by several experimental and theoretical investigations[6,19−24] that Cr^{3+} ions have a kinetically extremely inert first coordination shell containing six octahedrally coordinated water molecules with unusually long residence times of about 10^6 s[25] and, as a consequence, a second hydration sphere distinct from bulk water. The calculated $g_{Cr-OW}(r)$ and $g_{Cr-Cl}(r)$ are shown in Figure 3 for RedSy and ExtSy, respectively. The $g_{Cr-OW}(r)$ shows a sharp peak centered at ≈2.05 Å representing the first hydration shell, whereas the presence of a well-defined second hydration sphere is evidenced by a broader peak centered at about 4.24 Å. This peak is followed, in the ExtSy case, by another broad peak centered at ≈5.4 Å that could be ascribed to a diffuse third hydrations shell. As it can be noticed, the $g_{Cr-OW}(r)$ becomes zero after its first peak and remains almost zero for more than 1 Å, thus suggesting that the first hydration shell is very stable and that water exchange with the second shell is minimal, in agreement with experimental results and theoretical calculations.[6−8,26] Moreover, water molecules in the first shell are strictly oriented, pointing their oxygens toward the Cr^{3+} ions, thus confirming once again that the first coordination shell has a quite rigid structure. To evaluate the orientation of water molecules in the first and second hydration shells, the distributions of the θ angle ($\angle$H−O···Cr^{3+}) have been examined and are reported in Figure 4 for RedSy and ExtSy, respectively. A strong radial alignment for the first coordinated waters is apparent from the presence of a sharp and narrow peak centered at about 125°. The θ distributions of the second shell waters are, instead, much wider because of the higher mobility of these molecules which are exchanged with outer shell waters.

The mean coordination numbers of the first and second hydration shells of Cr^{3+} are 5.8 and 19.1, respectively, in both

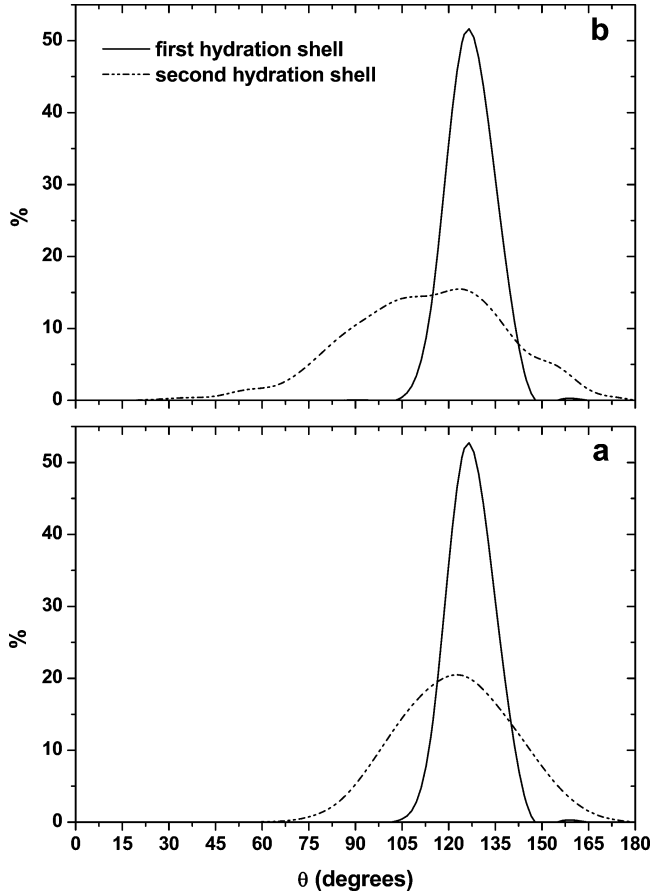

Figure 4. θ angle (H−O···Cr^{3+}) distributions of water molecules in the first (solid line) and second (dash−dot−dot line) solvation shells of the Cr^{3+} ions for (a) RedSy and (b) ExtSy.

the simulated systems. The number of water molecules in the second hydration shell is approximately three times as large as that in the first shell. Quite different coordination numbers for the second shell, 12 and 14, resulted, instead, from other theoretical simulations.[7] However, it must be pointed out that such comparisons are seldom straightforward. Coordination numbers can significantly depend on the concentration, on the presence of FLA molecules, on the water model employed, and on the chosen force field parameters, which are perhaps the most crucial aspect of the simulation studies.

The mean Cr^{3+}−Cl^- distance from our simulations is about 2.48 Å, signifying that Cl^- ions can be part of the Cr^{3+} first coordination shell. However, integration of the $g_{Cr-Cl}(r)$ between ≈2.2 and ≈2.7 Å gives a mean number of 0.5 and 3 Cl^- ions in the first sphere of each Cr^{3+} ion for RedSy and ExtSy, respectively. In the case of Cl^- ions, the two simulations produced different structural results; in fact, a second peak centered at 4.65 Å is visible in the $g_{Cr-Cl}(r)$ of RedSy, whereas only one peak is present in the ExtSy $g_{Cr-Cl}(r)$ plot. This fact can be explained considering the high concentration of ions and FLA molecules in the ExtSy simulation cell that causes Cl^- ions to be trapped near the positively charged Cr^{3+} ions.

The radial distribution functions $g_{Cr-O_i}(r)$ (i = 1, 3, 4, 7, 3′, and 4′) of the two simulations are plotted in Figure 5. In the RedSy case, there are only "long-range" structural correlations evidenced by diffuse peaks at distances longer than 4.2 Å with very small coordination numbers (the maximum value of 0.1 is found for O_4). These data suggest that Cr^{3+} ions are found in the second ill-defined coordination sphere of FLA oxygens and

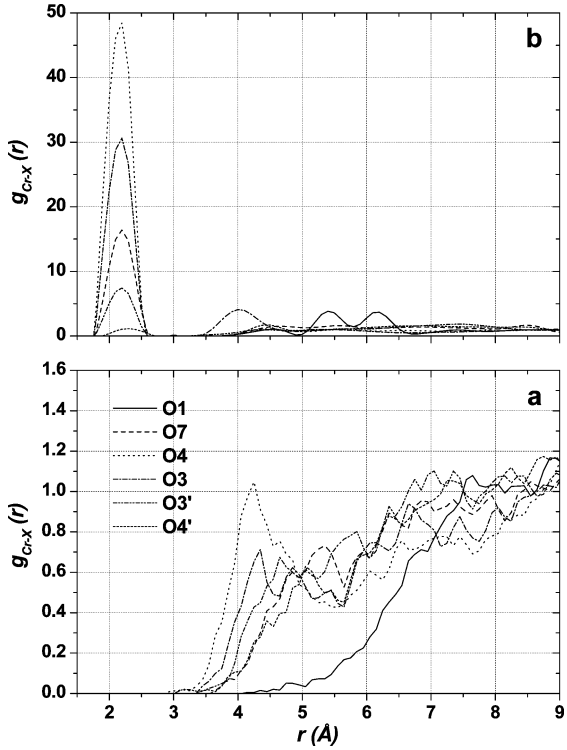

Figure 5. Cr^{3+}−FLA oxygen (O_i, i = 1, 3, 4, 7, 3′, and 4′) radial distribution functions for (a) RedSy and (b) ExtSy.

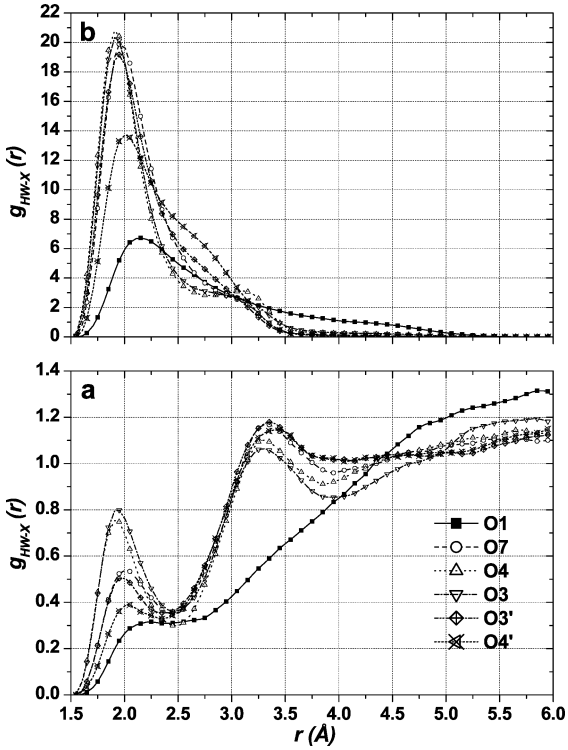

Figure 6. HW−FLA oxygen (O_i, i = 1, 3, 4, 7, 3′, and 4′) radial distribution functions for (a) RedSy and (b) ExtSy.

beyond, but their presence in the second shell is not statistically significant when only one FLA molecule is taken into account. However, from the collected results, it is possible to estimate which oxygen interacting sites the Cr^{3+} ions prefer, comparing the percentage of structures having a Cr^{3+} ion within 4.0 Å of each FLA oxygen. In agreement with the coordination numbers, O_4 was the most visited site with a population percentage of 1.7, followed by O_3, $O_{3'}$, O_7, $O_{4'}$, and O_1 with percentages of 0.8, 0.5, 0.4, 0.3, and 0.1. This difference in behavior can be attributed to both the atom's accessibility to solvent molecules and to its interactions with them. As a matter of fact, O_4 is exposed to the solvent and has a relatively high electrostatic charge (−0.6*e*) and, thus, stronger interactions with Cr^{3+} ions compared to O_1, which has a lower charge value (−0.2*e*) and, at the same time, is less reachable by the solvent. Notwithstanding, O_3 and $O_{3'}$ have the same atomic charge as O_4; their spatial positions and the possibility of intramolecular hydrogen bonds reduce their interacting capabilities. A similar behavior is manifested by the other oxygen atoms (O_7 and $O_{4'}$) which, in addition, have slightly lower charges (−0.5*e*). FLA partial charges can be found in the Supporting Information.

Contrarily to RedSy $g_{Cr-O_i}(r)$ plots, ExtSy Cr−O_3, Cr−O_4, Cr−O_7, Cr−$O_{3'}$, and Cr−$O_{4'}$ radial distribution functions have first narrow peaks at ≈2.2−2.3 Å, which represent ion−pair association, with related coordination numbers of 4.1, 6.4, 2.2, 1, and 0.2. At greater distances, lower and broader peaks with centers in the range 4.0−4.6 Å are noticeable as representatives of the second coordination shell. These features contrast with those of the O_1 radial distribution function, which, instead, displays two small peaks centered at ≈4.6 and ≈5.4 Å, with coordination numbers of 1.0 and 4.5, respectively.

As far as $g_{HW-O_i}(r)$ (i = 1, 3, 4, 7, 3′, and 4′) are concerned, collected data from the two simulations produced quite different radial distribution function plots (Figure 6). RedSy $g_{HW-O_i}(r)$ (i = 3, 4, 7, 3′, and 4′) (Figure 6a) show pronounced and narrow first solvation shell peaks with a maximum at 1.93 Å for O_3, at 1.92 Å for O_4, at 2.01 Å for O_7, at 1.98 Å for $O_{3'}$, and at 2.02 Å for $O_{4'}$ which integrate to around 1.2, 1.2, 1.0, 0.9, and 0.7 water molecules. Second more diffuse peaks centered at 3.29 for O_3, at 3.30 Å for O_4, at 3.32 Å for O_7, at 3.35 Å for $O_{3'}$, and at 3.42 Å for $O_{4'}$ are noticeable; their corresponding coordination numbers are the following: 9.0, 9.5, 11.5, 10.0, and 10.0. By contrast, $g_{HW-O_1}(r)$ displays only one small and broad peak at a slightly greater distance (≈2.24 Å) with a coordination number of about 0.5, indicating that the water around O_1 is the least structured among all six oxygens. The fact that $g_{HW-O_i}(r)$ do not go down to zero between the first and second hydration shell peaks suggests that these two shells easily interchange water molecules with each other during the whole simulation time. Instead, no distinct second solvation shell peaks are visible in the ExtSy HW−O_i radial distribution functions. Notwithstanding, ExtSy $g_{HW-O_i}(r)$ first hydration shell peaks are centered at the same distances as those found in the RedSy simulation; they show an asymmetric broadening which reflects a much less homogeneous distribution of the water throughout the system as confirmed by the decreased coordination numbers which are the following: 0.5 for O_1, 0.7 for O_3, 0.7 for O_4, 0.9 for O_7, 1 for $O_{3'}$, and 1 for $O_{4'}$.

The distribution of solvent species (water molecules and Cr^{3+} ions) around FLA was quantified by the FLA−WAT and FLA−Cr radial distribution functions which are displayed in Figure 7. The analysis has been focused on the comparison between solvation effects on the isolated molecule (RedSy) and solvation effects on self-aggregated structures immersed in a more concentrated ionic solution. Indeed, the radial distribution functions of five different FLA molecules, randomly chosen among the 57 molecules inserted in the ExtSy simulation cell, are compared with the RedSy corresponding one. The FLA−WAT radial distribution functions (Figure 7b) all have a similar trend, showing a first peak at ≈1.9 Å for the first solvation shell and a second peak with a maximum in the range 2.6−2.7 Å for the second hydration sphere. The coordination number

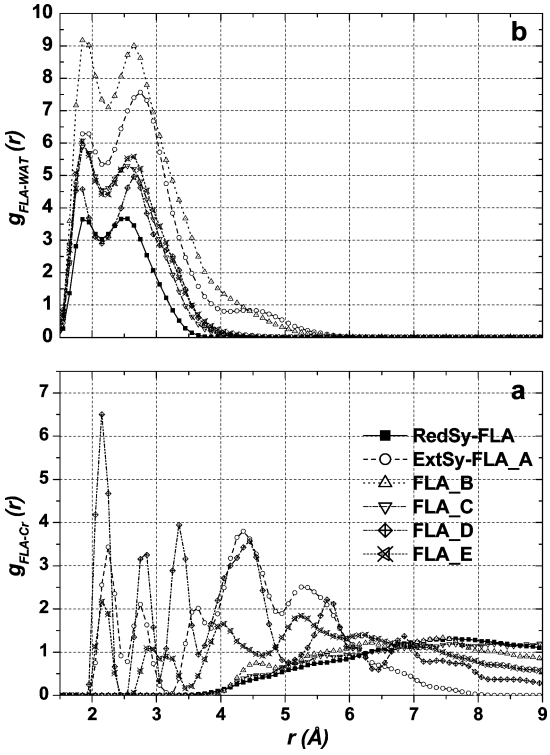

Figure 7. FLA−Cr (a) and FLA−WAT (b) radial distribution functions for RedSy and five different FLA molecules of ExtSy.

TABLE 1: Mean Residence Times (ps) for Water Molecules (WAT) and Cr^{3+} Ions around Each FLA Oxygen Atom

atom	0 WAT	1 WAT	2 WATs	3 WATs	4 WATs	1 Cr^{3+}
O_1	37	706	37			
O_3		56	161	241		4
O_4		89	181	156	92	7
O_7			179	462	129	3
$O_{3'}$			211	324	189	3
$O_{4'}$		260	199	308	218	2

corresponding to the first peak is 8 for the isolated molecule and structure C, whereas three different values (5, 6, 6, and 7) are obtained for the other conformations (A, B, D, and E). As it can be noticed, a different trend is apparent for $g_{FLA\_A-WAT}(r)$ which shows, beyond the second hydration shell, a broad peak centered at ≈4.5 Å, that could be described as a diffuse third hydration shell. Each plot integrates to around 35 water molecules. In contrast with the FLA−WAT radial distribution functions, which evidence similar structural results produced by the two simulations when FLA interacts with water, the FLA−Cr radial distribution functions reflect the diversity of the surrounding environment. The functions $g_{FLA\_A-Cr}(r)$, $g_{FLA\_D-Cr}(r)$, and $g_{FLA\_E-Cr}(r)$ (Figure 7a) show a series of well-defined peaks centered at different distances indicating the nearness of some Cr^{3+} ions to the solute, while, for the other cases, comprising the isolated FLA molecule of RedSy, Cr^{3+} ions are found farther away (more than 6 Å) from the solute atoms.

As it was expected, the two systems show different characteristics. Due to the fact that RedSy consisted of only one FLA molecule immersed in a more dilute solution, with respect to the ExtSy one, all its interacting sites are reachable by all the solvent species, whereas the presence of several FLA molecules in the same simulation box, in the ExtSy case, limits the accessibility of the FLA atoms to water molecules, Cr^{3+} and Cl^- ions. The formation of supramolecular aggregates, their size, and the nature of the self-interactions (hydrogen bonding and van der Waals interactions) are responsible for the different trend observed in the radial distribution function plots.

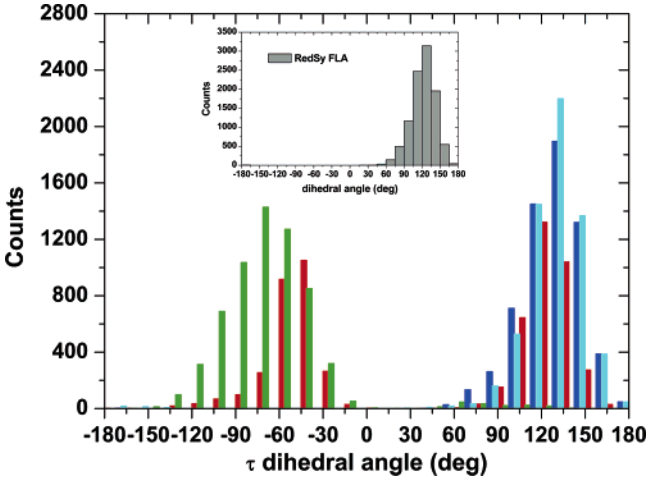

Figure 8. FLA τ dihedral angle distribution. Torsion angles of 4 different molecules randomly extracted from ExtSy are shown. The dihedral angle distribution of the RedSy FLA molecule is displayed in the inset for comparison.

3.2. Mean Residence Times. Solvent residence times were calculated by using the whole RedSy trajectory, where only one FLA molecule is present, and averaged out to obtain a mean residence time. Such values were calculated for FLA oxygen atoms to give an idea of the mobility of water and Cr^{3+} ions near those sites (Table 1). Water mean residence times (MRT) around each **FLA** oxygen were calculated considering only those water molecules within a distance of 3.3 Å from the examined sites, which roughly corresponds to the minimum in their radial distribution functions. Any water molecule that returned to this coordination shell after escaping for less than 5 ps was considered to be continuously bound to the atom under study, whereas any other molecule that was out of the shell for longer than 5 ps was regarded as a free molecule. The residence time of 0, 1, 2, 3, and 4 waters around each FLA oxygen was defined as the time each group of molecules spent near it. A similar definition was adopted for Cr^{3+} MRTs fixing a greater radius (4.0 Å) for the spherical region surrounding each oxygen. Careful examination of the data reported in Table 1 reveals, as expected, the greater tendency of hydroxyl oxygens (O_3, O_4, O_7, $O_{3'}$, $O_{4'}$) to interact with water molecules compared with the ring oxygen (O_1), which is less reactive due to its reduced electrostatic interaction energy, to the fact that it can only be a hydrogen bond acceptor, and to its uneasily reachable location considerably shielded by the bulky catechol side chain. The presence of nonzero water MRTs indicates an intense motion of solvent molecules between the coordination shells. All hydroxyl oxygens are always surrounded by at least one water molecule but up to four solvent molecules can be found within the cutoff distance with MRTs somewhat shorter than those observed for three neighboring waters. The O_7 atom is more exposed to the solvent than the other hydroxyl oxygens (the 3-water MRT is the longest one), which can be involved in intramolecular hydrogen bonds with each other and, thus, are less accessible to water molecules that, however, exchange extensively between the various solvation shells. Each oxygen site is more exposed to water than to chromium ions; in fact, Cr^{3+} MRTs are all shorter than 10 ps.

3.3. FLA Dihedral Angle Distributions. The dihedral angle distributions of α, β, γ, and τ were calculated for four different FLA conformations, randomly extracted from the ExtSy simulation run, and compared to the RedSy corresponding ones (Figure

TABLE 2: Hydrogen Bonds with a Percentage of Occupancy (% occ) Greater than 10%[a]

mol	atom	mol	atom	% occ	d_{ave}	d_{min}	σ_d	θ_{ave}	θ_{min}	σ_θ
3	$H_{O3'}$	**6**	O_4	16.8	2.88	2.52	0.16	14.10	7.16	0.27
3	H_{O4}	**7**	$O_{3'}$	15.1	2.88	2.52	0.16	17.30	7.19	0.71
3	H_{O3}	**17**	O_7	10.4	2.99	2.62	0.16	17.06	6.96	0.96
3	H_{O3}	**17**	O_4	35.9	2.82	2.50	0.14	13.66	6.94	0.38
5	H_{O7}	**10**	O_4	47.0	2.87	2.48	0.16	11.23	6.29	0.12
5	H_{O4}	**22**	O_3	19.6	2.87	2.51	0.16	12.92	6.93	0.36
6	H_{O7}	**7**	O_7	26.0	2.88	2.42	0.15	15.30	7.04	0.42
6	H_{O4}	**3**	$O_{3'}$	10.2	2.95	2.56	0.16	14.52	6.73	0.92
6	H_{O4}	**18**	$O_{4'}$	17.5	2.90	2.54	0.15	13.43	6.78	0.33
6	H_{O3}	**22**	O_4	12.5	2.91	2.58	0.16	13.95	7.13	0.22
7	H_{O7}	**11**	O_3	23.9	2.85	2.50	0.15	14.97	7.00	0.56
9	$H_{O3'}$	**5**	O_4	22.2	2.89	2.50	0.16	12.61	6.16	0.45
9	H_{O4}	**5**	O_7	37.7	2.96	2.53	0.16	14.88	7.06	0.49
9	H_{O3}	**2**	O_7	12.7	2.96	2.56	0.17	15.62	6.99	0.34
10	H_{O7}	**8**	O_3	49.9	2.82	2.44	0.15	13.43	6.82	0.24
11	H_{O3}	**10**	O_7	34.6	2.90	2.48	0.15	12.49	6.58	0.19
14	H_{O3}	**35**	O_7	16.0	2.86	2.51	0.15	21.36	5.51	4.06
16	H_{O7}	**3**	O_3	28.2	2.88	2.50	0.16	15.77	7.05	0.55
16	H_{O7}	**22**	O_3	12.6	2.88	2.53	0.16	12.77	6.82	0.67
17	H_{O3}	**21**	O_4	16.7	2.86	2.51	0.15	12.65	6.93	0.23
18	$H_{O3'}$	**3**	O_3	38.5	2.83	2.47	0.14	11.29	6.07	0.22
18	$H_{O3'}$	**16**	O_7	31.3	2.86	2.48	0.16	13.59	6.96	0.29
18	H_{O3}	**22**	O_7	11.4	2.97	2.56	0.16	17.04	7.12	0.76
21	H_{O7}	**18**	O_3	12.7	2.85	2.50	0.16	12.54	6.73	0.17
21	H_{O4}	**18**	O_3	31.1	2.89	2.52	0.16	13.58	6.92	0.27
22	H_{O3}	**6**	O_4	16.8	2.88	2.53	0.16	13.61	6.90	0.56
22	H_{O3}	**16**	O_7	14.6	2.96	2.58	0.17	16.46	7.57	0.61
26	$H_{O4'}$	**50**	O_4	13.4	2.84	2.52	0.16	13.55	6.85	0.43
26	H_{O3}	**1**	O_4	13.2	3.00	2.55	0.16	16.91	6.27	1.67
32	$H_{O3'}$	**33**	O_3	18.8	2.89	2.54	0.16	12.22	6.33	0.50
32	H_{O7}	**24**	$O_{4'}$	19.6	2.95	2.55	0.16	14.44	7.03	0.97
33	H_{O3}	**34**	O_3	14.0	2.87	2.55	0.15	15.13	7.00	0.72
37	H_{O7}	**35**	O_3	12.5	2.87	2.52	0.15	12.23	6.25	0.43
40	H_{O4}	**45**	O_7	13.7	2.89	2.56	0.16	16.59	7.00	0.53
42	H_{O4}	**43**	O_3	21.0	2.93	2.52	0.17	14.80	7.14	0.55
45	H_{O7}	**19**	O_3	33.0	2.84	2.52	0.15	13.60	6.56	0.14
45	H_{O7}	**40**	O_4	22.3	2.83	2.50	0.15	13.39	6.73	0.64
46	H_{O3}	**51**	O_3	11.3	2.88	2.54	0.16	14.22	7.01	0.32
47	H_{O3}	**50**	O_7	16.4	2.92	2.52	0.16	16.43	7.24	0.19
49	H_{O7}	**26**	$O_{4'}$	12.2	2.90	2.49	0.16	15.37	7.16	0.43
49	H_{O3}	**44**	O_3	27.7	2.88	2.53	0.16	17.33	7.23	0.55

[a] The molecule number (mol), atom name (atom), and the following statistical parameters are shown: average and minimum hydrogen−acceptor distances (d_{ave} and d_{min}), average and minimum hydrogen−donor−acceptor angles (θ_{ave} and θ_{min}), and distance and angle standard deviations (σ_d and σ_θ).

8). The distributions evidence the possible existence of several different conformations and thus the flexibility of the FLA structure in solution. The α, β, and γ hydroxyl dihedral angles change freely, during the whole simulation time, spanning the interval −180° to +180°, although the prominent angular domains correspond to in-plane values around 0° and ±180°, whereas the arrangement of the catechol side chain, defined by the τ torsion, is restricted to two dominant states. The first one has a distribution of values in the range −135°−15° with a maximum at about −58°, whereas the second one has values in the range 60°−180° with a maximum at about 130°. These findings are in agreement with the results previously obtained.[1]

In contrast, the Redsy FLA τ values, plotted in the inset, are distributed around a unique orientation (≈135°) with vanishingly small tails at about 60° and 180°. These results suggest that during the course of the simulation water activity alone is not sufficient to induce conformational changes involving the ring arrangement on a time scale of 10 ns and longer simulation times are probably necessary to observe such effects. However, when several FLA molecules are included in the system to be simulated, as was done in the ExtSy case and in our previous

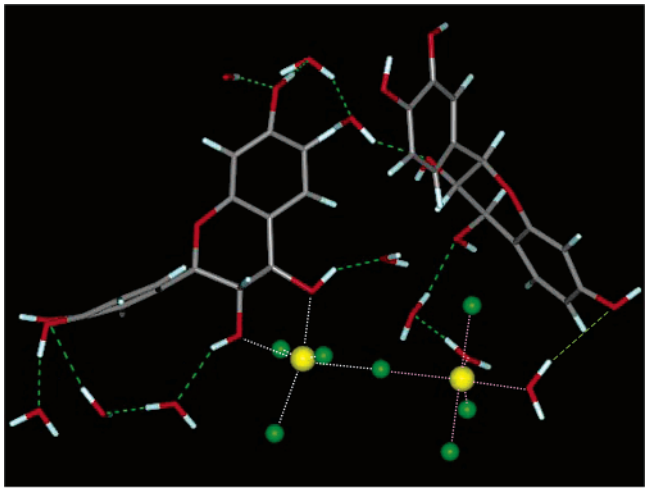

Figure 9. Portion of a trajectory snapshot showing two hydrogen bonded FLA molecules forming a complex (chelated structure) with Cr^{3+} ions (yellow spheres). Chlorine ions are displayed as green spheres, hydrogen bonds are represented as dashed green lines, and the Cr^{3+} coordination is evidenced by dotted white and pink lines.

MD calculations considering a collagenlike peptide segment surrounded by a mixed flavonoid/water solution, rearrangements of the catechol side chain are observed on time scales shorter than 2 ns. It can be only speculated that as a result of the interaction of FLA molecules with each other the catechol side chain is able to surmount the barrier separating its two characteristic orientations.

3.4. Hydrogen Bond Analysis and Molecular Aggregates. The structural organization and dynamics of FLA molecules are also correlated to the network of hydrogen bonds formed between them. The formation and breaking of these hydrogen bonds play an important role in determining the functionalities of these molecules which crucially depends on the number, *availability*, and location of their hydroxyl groups.[27]

Intermolecular hydrogen bonding interactions involving all of the five hydroxyl groups (O_3, O_4, O_7, $O_{3'}$, and $O_{4'}$), which can be, at the same time, hydrogen bond donors and acceptors, are responsible of the formation of complex supramolecular structures which are also held together by stacking interactions between the planar ring systems. The analysis of FLA−FLA hydrogen bonding characteristics during the simulation identified potential hydrogen bonds when donor−acceptor distances were smaller than 3.3 Å and the angle formed by the hydrogen donor−acceptor triplet was smaller than 30°. It is worth noting that if a sufficient number of acceptor sites were close enough to a donor atom and if the aforementioned criterion was satisfied a single donor could theoretically form more than one hydrogen bond at any given time. Details regarding long-lasting hydrogen bonds, i.e., those having a percentage of occupancy greater than 10%, found from the examination of the sampled configurations, are reported in Table 2. As it can be noticed, the H bond between O_7 and O_3 is the most persistent one, due to the fact that its percentage of occupancy is in each case above the chosen minimum (with a maximum of around 50 for the **8**···**10** dimer), and it has been detected in fourteen different FLA−FLA aggregates. Another persistent interaction is represented by the O_3···O_4 pair, where the maximum percentage of occupancy is ≈36% (**3**···**17** dimer) and eight bonded dimers are observed. All the other pairs (O_7···O_7, O_7···O_4, O_7···$O_{3'}$, O_7···$O_{4'}$, O_3···O_3, O_3···$O_{3'}$, O_4···$O_{3'}$, and O_4···$O_{4'}$) were involved in the formation of a lower number of molecular assemblies. By visual inspection, it has been noticed that water molecules contribute

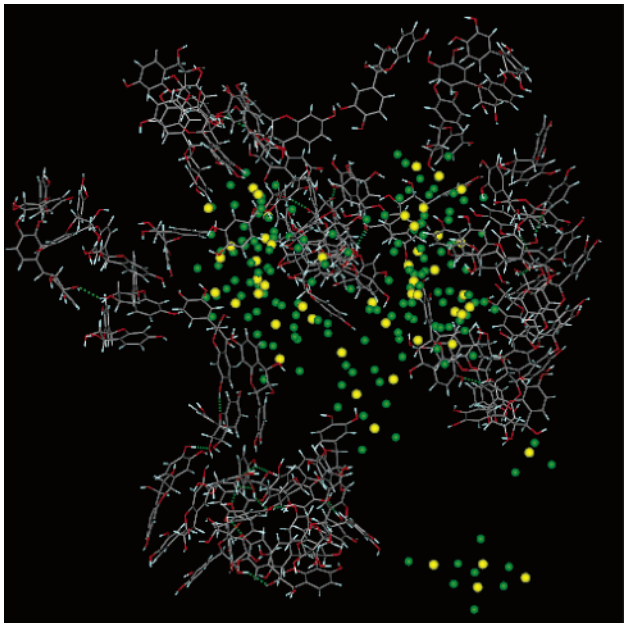

Figure 10. Trajectory snapshot showing the ExtSy simulation cell containing FLA aggregates, Cr^{3+} (yellow spheres) and Cl^{-} (green spheres) ions. Water molecules have been removed for clarity.

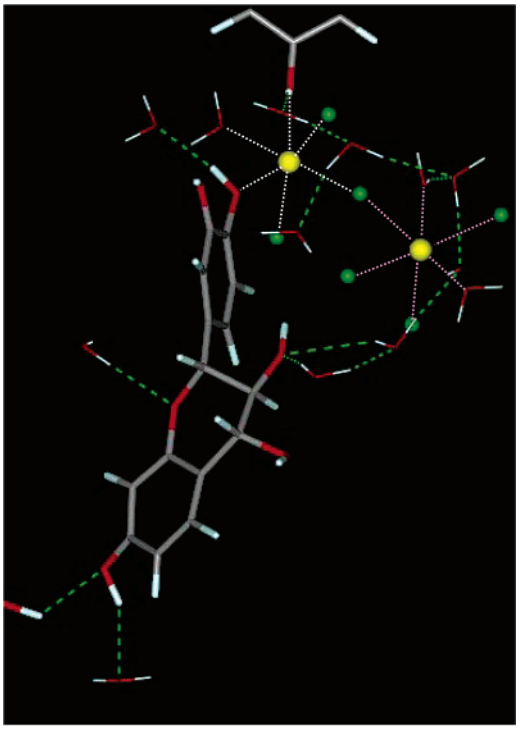

Figure 11. Subset of a trajectory snapshot showing one FLA molecule and a portion of the catechol side chain of another FLA molecule (top), forming a monocoordinated complex with a Cr^{3+} ion (yellow sphere). Chlorine ions are displayed as green spheres, hydrogen bonds are represented as dashed green lines, and the Cr^{3+} coordination is evidenced by dotted white and pink lines.

to the formation of the supramolecular systems by indirectly linking polyphenol molecules and thus causing each hydroxyl group of FLA to participate in the hydrogen bonding network that stabilizes the organic framework. Cr^{3+} ions together with Cl^{-} ions are part of these clusters (Figure 9). Most of FLA−Cr^{3+} aggregates are complexes with 1:1 stoichiometry where Cr^{3+} ions are preferentially located near the hydroxyl groups of the chromane ring system at a distance of about 2.1 Å from

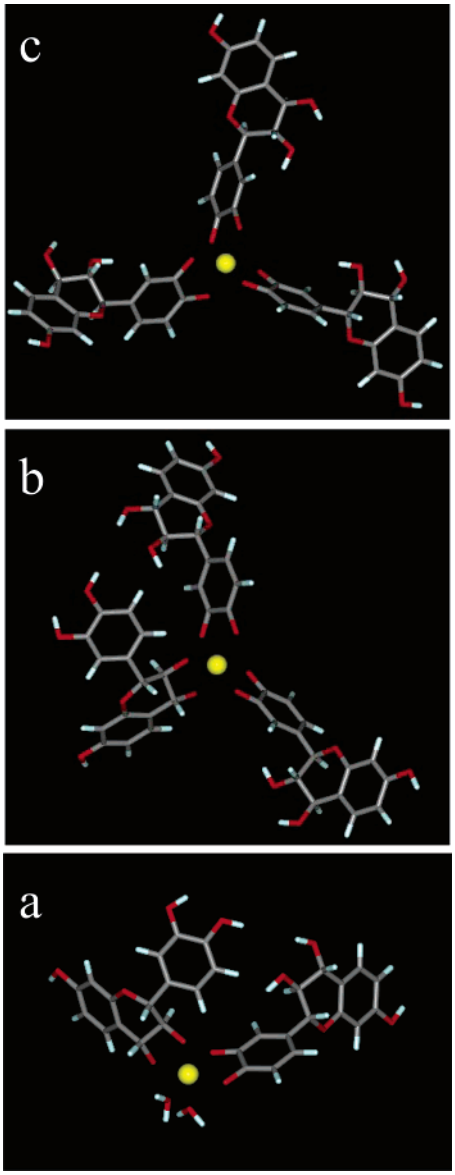

Figure 12. Extracted FLA−Cr^{3+} tri- and bimolecular complexes. (a) Mixed bimolecular chelated complex. Phenolyc and chromane hydroxyl groups are both involved, together with two water molecules, in Cr^{3+} coordination. (b) Mixed trimolecular chelated complex. Phenolyc and chromane hydroxyl groups are both involved in Cr^{3+} coordination. (c) Pure trimolecular chelated complex. Only phenolyc hydroxyl groups are involved in Cr^{3+} coordination. Hydrogens atoms of the coordinated hydroxyl groups have not been displayed for clarity reasons. The Cr^{3+} ion is represented as a yellow sphere.

each oxygen atom. As it appears from the inspection of Figure 9, which shows a portion of a trajectory snapshot (Figure 10), hydroxyl hydrogen atoms point in opposite directions, forming hydrogen bonds with surrounding water molecules, and the corresponding oxygen atoms are directly coordinated with a Cr^{3+} center, forming a chelated complex. In this particular example, as well as in other monocoordinated cases such as the one shown in Figure 11, in addition to the chromium mononuclear species, binuclear cations, in which Cr^{3+} ions are bridged by Cl^{-} ions, are visible. Several chromium clusters such as these and those with different coordinated structures have been found while analyzing the sampled data. Besides the chelated complex (Figure 9), another FLA molecule indirectly linked to the chelated FLA and to Cr^{3+} ions by a network of hydrogen bonded water molecules can be noticed in the picture, thus evidencing the important role played by water clusters in the stabilization

of supramolecular systems. The analysis of MD results has shown that Cr^{3+} binding takes place also through one or both of the phenolyc groups of the ligand molecule but to a minor extent (Figures 11 and 12). Moreover, in a limited number of geometries, four water ligands are replaced by two FLA molecules in the Cr^{3+} centers and sometimes all the coordinated waters are substituted by three polyphenol molecules (Figure 12).

4. Conclusions

The developed models used in this work to study the formation of supramolecular aggregates made by polyphenols, chromium(III) ions, chlorine ions, and water molecules have proven to be a valid and useful approach to predict and identify possible Cr^{3+} binding sites, to elucidate the role played by ions and water molecules in the stabilization of the complexes, and to establish a close relationship between the three-dimensional architectures of the self-assembled polyphenols and the number, location, and orientation of the hydroxyl groups present in the molecules. The computed results do not conflict with any of the experimental and theoretical data found in the literature; indeed, structural features regarding Cr^{3+} first and second hydration shells agree quite well with the experiment. The identified FLA$-Cr^{3+}$ complexes are in line with previous studies,[27−29] which report that metal chelators can sequester and coordinate metal ions through their hydroxyl groups, and the descriptions of the molecular aggregation and self-aggregation mechanisms are quite reasonable and in agreement with experimental findings.[27,30] The structure of the sampled clusters is characterized by long-range space correlations that reflect the nature of the interaction energy mainly dominated by electrostatic contributions, thus resulting in a charge ordering effect. Although the computed structures qualitatively capture the essential feature of the interaction, the observed substitutions of Cl^- ions and water molecules from the Cr^{3+} coordination sphere by the FLA ligand molecules through complex formation and chelation should be further investigated in detail by using longer simulations and higher-level calculations in order to properly understand and to quantify the correlation between polyphenol activity and the function, structure, and dynamics of FLA molecules and the surrounding environment. These later aspects are currently under investigation and will be presented in a forthcoming paper.

Acknowledgment. Most of the calculations reported in this paper were done on the resources of the Cineca supercomputer center made available to us through the "INFM−Iniziativa Trasversale Calcolo Parallelo 2004 and 2005".

Supporting Information Available: FLA molecule structure and partial charges. This material is available free of charge via the Internet at http://pubs.acs.org.

References and Notes

(1) Cappelli, C.; Bronco, S.; Monti, S. *Chirality* **2005**, *17*, 577−589.
(2) McDonald, M.; Mila, I.; Scalbert, A. *J. Agric. Food Chem.* **1996**, *44*, 599−606.
(3) Covington, A. D. *Chem. Soc. Rev.* **1997**, *26*, 111−126.
(4) Bronco, S.; Cappelli, C.; Monti, S. *J. Phys. Chem. B* **2004**, *108*, 10101−10112.
(5) Monti, S.; Bronco, S.; Cappelli, C. *J. Phys. Chem. B* **2005**, *109*, 11389−11398.
(6) Blenzen, A.; Foglia, F.; Furet, E.; Helm, L.; Merbach, A. E.; Weber, J. *J. Am. Chem. Soc.* **1996**, *118*, 12777−12787.
(7) Pappalardo, R. R.; Martínez, J. M.; Marcos, E. S. *J. Phys. Chem. B* **1996**, *100*, 11748−11754.
(8) Kritayakornupong, C.; Yagüe, J. I.; Rode, B. M. *J. Phys. Chem. A* **2002**, *106*, 10584−10589.
(9) Imer, S.; Varnali, T. *Appl. Organomet. Chem.* **2000**, *14*, 660−669.
(10) Grubišić, S.; Gruden, M.; Niketić, S. R.; Sakagami-Yoshida, N.; Kaizaki, S. *J. Mol. Struct.* **2002**, *609*, 1−9.
(11) Grubišić, S.; Gruden-Pavloviæ, M.; Niketić, S. R.; Sakagami-Yoshida, N.; Kaizaki, S. *Transition Met. Chem.* **2003**, *28*, 37−42.
(12) Case, D. A.; et al. *AMBER 8*; University of California: San Francisco, CA, 2002.
(13) Sabolović, J.; Mrak, Z.; Koštrun, S.; Janeković, A. *Inorg. Chem.* **2004**, *43*, 8479−8489.
(14) Bol, W.; Welzen, T. *Chem. Phys. Lett.* **1977**, *49*, 189−192.
(15) Frisch, M. J.; et al. *Gaussian 03*, revision A.1; Gaussian, Inc.: Pittsburgh, PA, 2003.
(16) Jorgensen, W. L. *J. Am. Chem. Soc.* **1981**, *103*, 335−350.
(17) Ryckaert, J. P.; Ciccotti, G.; Berendsen, H. J. C. *J. Comput. Phys.* **1977**, *23*, 327−341.
(18) Berendsen, H. J. C.; Postma, J. P. M.; vanGunsteren, W. F.; DiNola, A.; Haak, J. R. *J. Chem. Phys.* **1984**, *81*, 3684−3690.
(19) Ohtaki, H.; Radnai, T. *Chem. Rev.* **1993**, *93*, 1157−1204.
(20) Lindqvist-Reis, P.; noz Páez, A. M.; Diáz-Moreno, S.; Pattanailk, S.; Persson, I.; Sandström, M. *Inorg. Chem.* **1998**, *37*, 6675−6683.
(21) Sakane, H.; noz Páez, A. M.; Diáz-Moreno, S.; Martínez, J. M.; Pappalardo, R. R.; Marcos, E. S. *J. Am. Chem. Soc.* **1998**, *120*, 10397−10401.
(22) Floris, F.; Persico, M.; Tani, A.; Tomasi, J. *Chem. Phys.* **1995**, *195*, 207−216.
(23) Martínez, J. M.; Hernández-Cobos, J.; Saint-Martin, H.; Pappalardo, R. R.; Marcos, E. S. *J. Chem. Phys.* **2000**, *112*, 2339−2347.
(24) Bergstrom, P. A.; Lindgren, J.; Read, M.; Sandstrom, M. *J. Phys. Chem.* **1991**, *95*, 7650−7655.
(25) Cusanelli, A.; Frey, U.; Richens, D. T.; Merbach, A. E. *J. Am. Chem. Soc.* **1996**, *118*, 5265−5271.
(26) Helm, L.; Merbach, A. E. *Coord. Chem. Rev.* **1999**, *187*, 151−181.
(27) Rossi, M.; Meyer, R.; Constantinou, P.; Caruso, F.; Castelbuono, D.; O'Brien, M.; Narasimhan, V. *J. Nat. Prod.* **2001**, *64*, 26−31.
(28) Fresen, M.; Pommier, Y.; Leteurtre, F.; Hiroguchi, S.; Jung, J.; Kohn, K. W. *Biochem. Pharmacol.* **1994**, *48*, 595−608.
(29) Hider, R. C.; Liu, E. D.; Khodr, H. H. *Methods Enzymol.* **2001**, *335*, 190−203.
(30) Poncet-Legrand, C.; Cartalade, D.; Putaux, J.-L.; Cheynier, V.; Vernhet, A. *Langmuir* **2003**, *19*, 10563−10572.